European Polymer Journal 115 (2019) 364–374

Contents lists available at ScienceDirect

European Polymer Journal

journal homepage: www.elsevier.com/locate/europolj

Polyurethane synthesis under high-pressure CO_2, a FT-NIR study

Maria Rosaria Di Caprio[a,1], Cosimo Brondi[a,1], Ernesto Di Maio[a,*], Thomas Mosciatti[b], Sara Cavalca[b], Vanni Parenti[b], Salvatore Iannace[c], Giuseppe Mensitieri[a], Pellegrino Musto[d]

[a] Dipartimento di Ingegneria Chimica, dei Materiali e della Produzione Industriale, University of Naples Federico II, P.leTecchio 80, 80125 Naples, Italy
[b] Dow Italia s.r.l, Polyurethanes R&D, via Carpi 29, 42015 Correggio, Italy
[c] Institute for Macromolecular Studies, National Research Council, Via Edoardo Bassini, 15, 20133 Milan, Italy
[d] Institute on Polymers Composites and Biomaterials, National Research Council, Via Campi Flegrei, 34, 80078 Pozzuoli, Italy

ARTICLE INFO

Keywords:
Polyurethane
CO_2
FT-NIR spectroscopy
Sorption
Synthesis

ABSTRACT

The effect of CO_2 on the polyurethane synthesis between a polyol and an isocyanate was studied by in situ near infrared spectroscopy in a newly developed instrumented foaming equipment. In particular, first two solutions, namely a polyol/CO_2 solution and an isocyanate/CO_2 solution were formed at high pressure and then, upon mixing, the synthesis was promoted, still under pressure. Near infrared spectroscopy in reflection mode was used to monitor both CO_2 sorption in the polyol and in the isocyanate and the polyurethane synthesis under pressure. Results revealed a significant slowing down effect by the sorbed CO_2, apparently due to two concurrent mechanisms, namely catalyst deactivation and dilution.

1. Introduction

In the processing of thermosetting polyurethane foams (PUs), the nature and the amount of the blowing agents have a fundamental role in defining the cellular structure and, in turn, the properties of the foam. Since the introduction of PUs at the beginning of last century until the late 1950 s, CO_2 derived from the blowing reaction of isocyanate with water has been used as a blowing agent [1]. Here, water is the chemical blowing agent (CBA) and CO_2 is the product of the blowing reaction, which is concurrent to the polyurethane synthesis reaction. CO_2 does not, in fact, solubilize in the polyol and the isocyanate phases prior to foaming: conversely, it gradually forms and inflates the bubble at relatively low pressures. Large PUs production also utilized chlorofluorocarbons (CFCs) (in the late 1950 s) and hydrochlorofluorocarbons (HCFCs) (at the beginning of 1990 s) as physical blowing agents (PBAs), then replaced by hydrocarbons (HCs) (e.g. pentane) because of their negative environmental impact [1]. PBAs, differently from CBA, are mixed at ambient temperatures and pressures to form liquid solutions with the polyol and/or isocyanate phases and then become available in the gaseous state when the system is brought to super-saturation conditions, typically by the temperature rise following the exothermic synthesis reaction. Although cheap and with zero ozone depletion potential (ODP), HCs use was limited by their inherent flammability [1]. In this context, CO_2 is considered more sustainable and safer, with zero ODP and the lowest global warming potential (GWP = 1) among known blowing agents [1]. As a drawback, CO_2 solubility is lower than HCs and, in order to reach concentrations suitable for foaming, high pressures have to be utilized, thereby increasing the processing complexity. High-pressure CO_2 foaming, however, proved very effective with thermoplastics, where utmost performances in terms of cell number densities have been reached: microcellular and, more recently, nanocellular foams have been produced, characterized by improved thermal insulating and mechanical properties as compared to standard cell-sized foams [2]. So far, thermosetting foams stay orders of magnitude behind, in terms of cell size.

Because of the environmental concerns and of the encouraging performance in producing microcellular and nanocellular foams with thermoplastic polymers, CO_2 has most recently attracted a growing industrial interest as a PBA for PUs [3]. In order to use CO_2 as a PBA (to be solubilized at high-pressure in the polyol and/or isocyanate) in polyurethane foaming, it is fundamental to understand the behavior of the reacting system in the presence of CO_2. In particular, CO_2 may play a critical role in the different reactions involved in the polyurethane synthesis.

The effect of the CO_2 presence (in particular, in supercritical conditions) in a reacting system has been largely reported in the literature, resulting an additional parameter to manipulate reaction kinetics. For instance, Stassin et al. [4] reported the effect of CO_2 in supercritical

* Corresponding author.
E-mail address: edimaio@unina.it (E. Di Maio).
[1] Authors contributed equally to this work.

https://doi.org/10.1016/j.eurpolymj.2019.03.047
Received 18 December 2018; Received in revised form 22 March 2019; Accepted 24 March 2019
Available online 25 March 2019
0014-3057/

conditions on the kinetics of ring-opening polymerization of ε-caprolactone. Authors observed a slowing down of the polymerization reaction, ascribed to the occurrence, in presence of CO_2, of a carbonation reaction responsible for a positive volume of activation and a higher energy of activation as compared to polymerization in a regular hydrocarbon solvent. In particular, the tin alkoxide initiator responsible for the growth of the polycaprolactone chains was carbonated by compressed CO_2, as verified by infrared spectroscopy. Tiltscher et al. [5] showed that catalyst deactivation occurred during a gas-phase reaction, when hexene oligomers with low volatilities deposited on the catalytically active surface. Performing the reaction at the same temperature, but above the critical pressure prevented the deposition of these oligomers and the ensuing catalyst deactivation. The readiness of CO_2 to interact chemically with proton-containing nucleophiles, such as water, alcohols and primary, secondary and tertiary amines was used to develop switchable systems [6,7]. The reversible binding between CO_2 and primary, secondary and tertiary amines is well known in literature, for example in CO_2 capture processes [8–10] and it has been shown of potential interest in other areas such as in catalytic processes, where CO_2 is simultaneously used as solvent and as a protecting group for amines. Examples include the ring closing metathesis and the hydroaminomethylation of secondary amines [11,12] . Only a few studies have been reported so far on the effect of high-pressure CO_2 on polyurethane synthesis. A hint to the retardation effect by CO_2 on PU synthesis is given in a patent on the effect of a specific surfactant on the properties of a PU foam [13], whereas, in a paper on PU foaming by high-pressure CO_2 [14], it was found that the time needed to reach adequate viscosities for foaming increased significantly with CO_2 content in the reacting system.

In the attempt to use high pressure CO_2 as a PBA in PUs foaming, a throughout and scientifically grounded study has to include the following ingredients: (i) sorption thermodynamics and mass transport properties of the CO_2 with both the polyol and the isocyanate; (ii) the effect of the CO_2 concentration on the PUs synthesis kinetics; (iii) a new processing procedure to cope with the two very different time scales of the foaming O(0.01–1s) (O order of magnitude) and the gelling reaction O(1–10 min). The usual PUs synthesis, in fact, occurs via the concurrent blowing and gelling reactions O(1–10 min), while foaming by pressure quenching the PBA is much faster (as faster as possible to decrease bubble size). In this context, sorption thermodynamics and mass transport properties have been reported in [15,16], while this work deals with the effect of CO_2 on the different reactions involved in the PUs synthesis. A new processing procedure has been recently introduced and will be the object of a forthcoming paper.

In this paper, we present the use of FT-NIR spectroscopy in diffuse reflection mode both to monitor in situ CO_2 sorption and the curing under CO_2 pressures of a polyurethane formulation. To do so, we adopted an instrumented pressure vessel, recently introduced by our group purposely to study polyurethane foaming by high-pressure CO_2 [17].

2. Experimental

2.1. Materials

A polyether polyol (Table 1) and polymeric methylene diphenyl diisocyanate (PMDI) (Table 2) were supplied by DOW Chemical Italy S.r.L. (Correggio, RE, Italy) within the LIFE13-ENV/IT/001238 project [3] and used “as received”. In particular, tertiary amine-based catalysts were included within the polyol formulation (e.g. Pentamethyldiethylenetriamine and Dimethylcyclohexylamine). High purity grade CO_2 (99.95% pure) was supplied by SOL (Naples, Italy).

2.2. Experimental set-up

As described in details in [17], in situ FT-NIR spectroscopic investigation of CO_2 sorption and polyurethane curing were conducted by using Frontier™ NIR spectrometer (Perkin Elmer Inc., Waltham, MA, USA) equipped with a tungsten halogen source, a CaF_2 beam splitter, a FlexIR™ NIR Fiber Optic reflectance probe (PIKE Technologies, Inc., Madison, WI, USA) and an InGaAs detector. The probe was housed beneath a high-pressure-tight sapphire window (Precision Sapphire Technologies, Vilnius, Lithuania) placed on the bottom plate of a 1 L pressure vessel (Fig. 1a and 1b). The sapphire window was in contact with an optical glass cylindrical sample holder, placed inside the pressure vessel, containing the polyol or the PMDI, kept separate by a rubbery impeller, during the CO_2 sorption test. The rubbery impeller, after sorption, is allowed to mix the two reactants by a lab mixer connected to the impeller via a high-pressure bearing, to study curing under pressure. This experimental set-up has been recently introduced by some of the authors and represents an unique experimental tool to thoughtfully study polyurethane foaming under high pressure [17]. It is worth of note that, as the PU reactions are exothermal, some degree of non-isothermicity cannot be excluded. In this framework, the presence of solubilized CO_2 affects the reaction kinetics, as observed, and the heat capacity of the reacting medium, as well, in turn affecting the temperature evolution of the system. Both factors contribute concurrently to the diminishing of the temperature rise by reaction as the amount of solubilized CO_2 increases. The experimental apparatus is not designed, in the present configuration, to measure the temperature profile evolution of the reacting matter, which could be an important point for further development.

2.2.1. Sorption

Raman spectra of neat PMDI and PMDI/CO_2 solution at a CO_2 pressure of 2 MPa and 35 °C were collected in order to investigate possible interactions between the PMDI and the dissolved CO_2. After 16 h-contact, neither peak shift nor peak modification of the PMDI/CO_2 solution with respect to the neat PMDI were detected, revealing that no interaction or reaction occurred (data not reported).

During the sorption tests, the polyol (or the PMDI) was poured in the glass cylindrical sample holder, and a metal reflector (with a path length of approximately 0.5 mm) was placed on top of the sample (Fig. 1c). The two reactants are lightly colored transparent viscous liquids and the reflector is necessary in order to return the near-infrared

Table 1
Composition of the polyether polyol.

Components	Molecular weight (Mw) (Da)	Functionality (f)	Parts (%)
Glycerin initiated polyether polyol	1000	Low	95
Amine initiated polyether polyol	500	High	
Sorbitol initiated polyether polyol	700	High	
Sucrose/glycerin initiated polyether polyol	500	High	
Catalysts	/		3
Surfactant	/		2

Polyol contains 0.2% water and polydispersity index (PDI) is 1–1.5; viscosity = 15150 mPa.s (25 °C); data from the supplier.

Table 2
Properties of the PMDI.

Component	Equivalent weight	NCO content (%)	Functionality	Viscosity mPa.s (25 °C)	Acidity as %HCl
PMDI	135	31.1	2.7	190	0.02

Data from the supplier.

light to the collecting probe (transflectance sampling). The sample holder is then placed in the pressure vessel onto the sapphire window (Fig. 1d) and then the pressure vessel is closed. After reaching the testing temperature, in this case 35 °C, CO_2 pressure is increased up to the saturation pressure (in the range from 0 to 4000 kPa) and kept for a sufficient amount of time, until equilibrium.

FT-NIR spectra were recorded automatically at regular time interval of 5 min using Perkin Elmer TimeBase software, in the spectral range 4000–10000 cm^{-1} with a resolution of 4 cm^{-1} and 32 scans. It is worth of note, here, that sorption monitoring by infrared spectroscopy has been already reported [18] and requires, for a quantitative analysis, calibration by known concentrations. In our case, we measured sorption by a coupled gravimetry-axisymmetric drop shape analysis (see Ref. [19] for the details) on the two reactants, as reported in Refs. [15,16]. The FT-NIR acquisitions allowed us to detect the combination bands as due to CO_2 sorption. The area under the monitored peaks was integrated and directly correlated to the amount of CO_2 sorbed in the polymer according to Beer-Lambert Law through univariate analysis by using Perkin Elmer TimeBase software. Subtraction of the spectrum of the initial reactant (polyol or PMDI), with no dissolved CO_2, from all of the spectra allowed to remove the contribution of other bands that overlap with the combination band of CO_2. Further details on the calibration method for quantitative evaluation are reported in Section 3.1.

2.2.2. Curing

In order to monitor the PU curing, polyol and PMDI (1:1.15 by weight) were gently cast in the sections of a glass cylindrical sample holder formed by the sample holder itself and the blades of a rubber impeller, which prevents the premature mixing of the two reactants (see Fig. 1e). The sample holder was then placed in the pressure vessel onto the sapphire window and secured by the Teflon coupling (see Fig. 1f). The pressure vessel is then pressurized and sorption is conducted for a defined period. After sorption, the two reactants are mixed for the reaction to occur by operating the impeller with a mixing shaft connected to a lab mixer by a high-pressure bearing [17]. The curing reaction was conducted, still under pressure, for a suitable amount of time, until completion.

The curing reaction, at several CO_2 pressures and 35 °C, was monitored by collecting spectra automatically at regular time interval of 20 s (*fast NIR monitoring*) with a resolution of 4 cm^{-1} and 8 scans, after mixing at 250 rpm for 10 s until the end of the curing.

Various implementations of vibrational spectroscopy have been successfully applied to study heterogeneous catalytic reactions with the objective of identifying intermediates and determining catalytic reaction mechanisms involved in the polyurethane synthesis [20]. In the field of synthesis under CO_2, when polyurethane synthesis is monitored by FT-NIR spectroscopy, it is possible to detect, among others, the NCO band decrease and the NH band (of the urethane group) formation and increase allowing for a quantitative analysis of the curing process [21].

In order to meter a known CO_2 amount in the two PU formulation components, sorption time as well as CO_2 pressures were varied. The total CO_2 amount sorbed within the two phases (PMDI and polyol, separate by the rubbery impeller, see Fig. 1e) at a certain CO_2 pressure after a given sorption time was calculated by assuming: (i) a Fickian behavior for the two phases, (ii) constant thickness and gas diffusivities (PMDI/CO_2 and polyol/CO_2 mutual diffusivities) and (iii) one-dimensional transport problem (sorption occurs by diffusion through the top surface, while no flux is assumed to occur at bottom and lateral surfaces) [22]. Solubility and diffusivity data were gathered, for the two compounds, in [15,16]. With these assumptions, the well-known error function describes the CO_2 concentration profiles as a function of time elapsed after instantaneous pressurization. The average CO_2 fraction at each sorption time, for each phase, can be calculated after integration of said profiles. When mixing the two CO_2-laden fluids (a polyol/CO_2

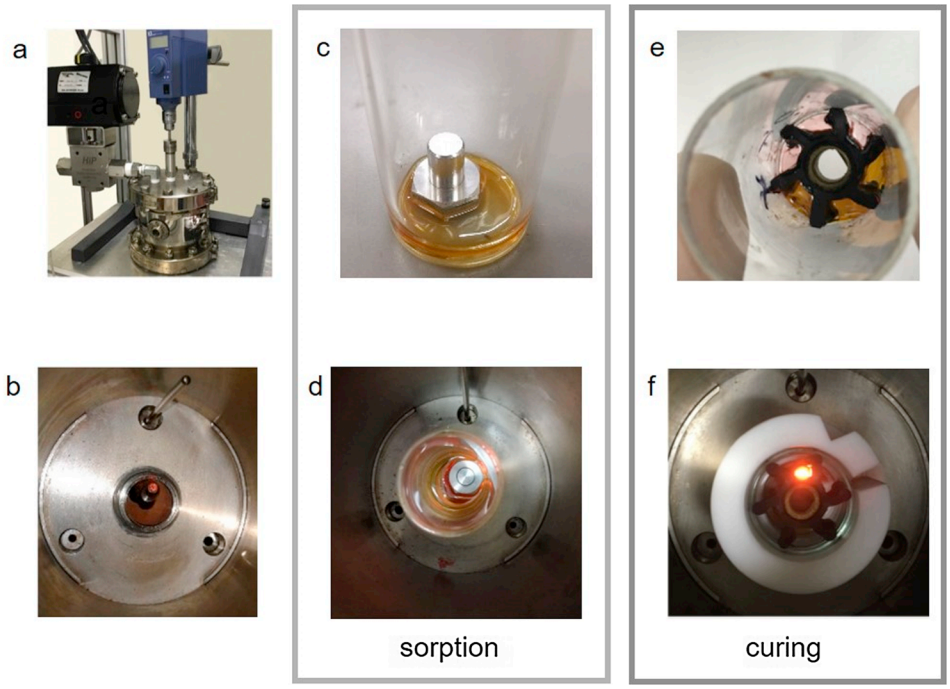

Fig. 1. Pictures of the adopted instrumentation. (a) Assembly of the high-pressure PU foaming equipment, showing the mixing head and the gas evacuation system; (b) detail of the probe and the sapphire windows placed at the bottom plate of the pressure vessel (top view). (c) and (d) set up for the sorption tests (light gray box): (c) sample holder with the polymer (PMDI in this image) and the reflector and (d) positioning of said sample holder inside of the pressure vessel. (e) and (f) set up for the curing tests (dark gray box): (e) sample holder with the rubbery impeller that keeps separate the two reactants for sorption and (f) details of the Teflon coupling of the sample holder with the sapphire window; the light comes from the NIR probe. See [17] for details.

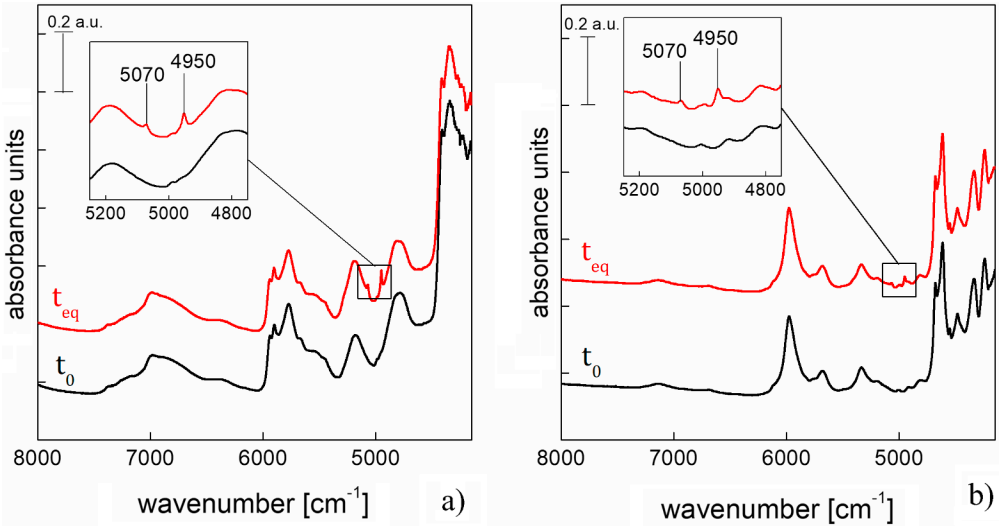

Fig. 2. FT-NIR spectra of (a) polyol and (b) PMDI before (black line) and after (red line) exposure for 3 days at CO_2 at 4000 kPa and 35 °C. The inset shows a detailed view of the two CO_2 combination bands at 4950 and 5070 cm^{-1}. Spectra are shifted vertically for clarity. (For interpretation of the references to colour in this figure legend, the reader is referred to the web version of this article.)

solution and a PMDI/CO_2 solution), the PU synthesis reaction is allowed to start. Due to the different time scales of sorption O(10 h) and of reaction O(10 min), we assumed the sorption that may occur after mixing negligible. Furthermore, immiscibility of the components excludes the possibility of CO_2 exclusion upon mixing [23]. Hence, the average CO_2 weight fraction in the reacting mixture, $\bar{w}_{CO_2}$, was calculated by weight-averaging the CO_2 fractions sorbed within the two phases before mixing [22].

3. Results and discussion

3.1. Sorption

FT-NIR spectra of polyol and PMDI before and after exposure for three days at 4000 kPa of CO_2 and 35 °C are reported in Fig. 2a and b, respectively. Sorption time was selected, based on diffusivity data [15,16] and on the sample amount, to attain equilibrium. According to previous studies [24], FT-NIR spectra of pure CO_2 show combination bands due to the coupled Fermi resonance. In Fig. 2, spectra of the samples exposed to CO_2 reveal combination bands at 4950 cm^{-1} ($\nu_1 + 2\,\nu_2 + \nu_3$) and 5070 cm^{-1} ($2\,\nu_1 + \nu_3$) [24]. In the following, the combination band at 4950 cm^{-1} is selected to estimate, via the Beer-Lambert law and by using gravimetric data retrieved in [15,16], the amount of CO_2 sorbed in the polymeric phases [18].

The detailed time-evolution of FT-NIR spectra of CO_2 sorption monitoring in the polyol, at 4000 kPa and 35 °C, and the difference spectra are reported in Fig. 3(a) and (b). Fig. 3c reports the evolution of the integrated area under the combination band of CO_2 (A_{CO2}) at 4950 cm^{-1}. A_{CO2} attains equilibrium after ca. three sorption days and the equilibrium value, A^{eq}_{CO2}, can be evaluated as the average value of the final plateau. Assuming a linear dependence (Beer-Lambert law) between A_{CO2} and weight fractions of the CO_2 [25] and the sample thickness, L, constant, FT-NIR kinetics data can be utilized to calculate the mutual polyol/CO_2 diffusivity, D, by fitting data with the first term approximation of the Fickian model [26]:

$$\ln\left(1 - \frac{A_{CO2}}{A^{eq}_{CO2}}\right) = \ln\left(\frac{8}{\pi^2}\right) - \frac{D\pi^2 t}{L^2} \quad (1)$$

The evaluation of the limiting slope of $\ln\left(1 - \frac{A_{CO2}}{A^{eq}_{CO2}}\right)$ vs. t for the different tests conducted on both the polyol and PMDI at different pressures and at 35 °C allowed to measure D of $1.01{\cdot}10^{-6}$ cm^2/s for the polyol/CO_2 system and of $2.3{\cdot}10^{-6}$ cm^2/s for PMDI/CO_2 at 4000 kPa, in agreement with those retrieved with coupled gravimetry – ADSA [15,16]. It is worth of note, here, that evaluation of diffusivity by the above method does not require any calibration with actual weight fraction data (just the assumption of validity of the Beer-Lambert law).

To use spectral information as a quantitative tool for CO_2 sorption, a calibration was performed based on data gathered with coupled gravimetry – ADSA [15,16]. The procedure is described in Fig. 4, where, for both polyol and PMDI, A^{eq}_{CO2} values at 2000 and 4000 kPa and 35 °C are reported as function of CO_2 sorption pressure. Data draw a linear dependence with pressure, which can be described as $A^{eq}_{CO2} = m \bullet P_{CO2}$ where m is equal to $2.68{\cdot}10^{-4}$ cm^{-1}/kPa for polyol and $1.53{\cdot}10^{-4}$ cm^{-1}/kPa for isocyanate. This result allows us to interpret curing results in a more consistent way, as it will be seen in the following. The inset in Fig. 4 shows A^{eq}_{CO2} vs. $\bar{w}_{CO_2}$, collectively for both the polyol and PMDI. Data fit nicely on a single line, proving that molar absorptivity of CO_2 is not affected by the specific polymeric phase. This is an important conclusion, that allows a more rigorous treatment of IR data, as it will be shown in the following.

3.2. Curing

The measurement of the effect of the different CO_2 concentrations on the polyurethane curing reaction kinetics is the primary objective of the present study, where FT-NIR is utilized to monitor the different isocyanate reactions taking place simultaneously in the standard PUs formulations [27]. In particular, in the formulation utilized in the present study, the following reactions take place: (i) the isocyanate and the hydroxyl group react to give a carbamate ("urethane" in case of high molecular weights) as the desired product; (ii) the isocyanate reacts with water to produce a carbamic acid, which breaks down into carbon dioxide and a primary amine that reacts immediately with another isocyanate to form urea; (iii) three isocyanates react together to give an isocyanurate (trimerization). For the sake of clarity, the chemical CO_2 produced by the blowing reaction was considered negligible in comparison with the CO_2 dissolved within the two phases (polyol and isocyanate) during the sorption stage. Hence, the isocyanate, characterized by the NCO group, readily detectable by NIR, is involved in different reactions and may be utilized to describe an overall reaction rate, by following its consumption. Furthermore, the isocyanate and the polyol react together (i) to produce PU which is characterized by the NH(CO)O group where the NH vibration is also readily detectable by NIR [21]. The PU production rate is, hence, quantifiable as well. To this aim, collected spectra can be treated as described by the help of Fig. 5, reporting the spectra of the single reactants/CO_2 solutions (a and b), collected before mixing (after 5 h of sorption time), a spectrum collected right after mixing the two components at 250 rpm for 10 s (c) and a spectrum collected at the end of the curing reaction (after 2h, d). In

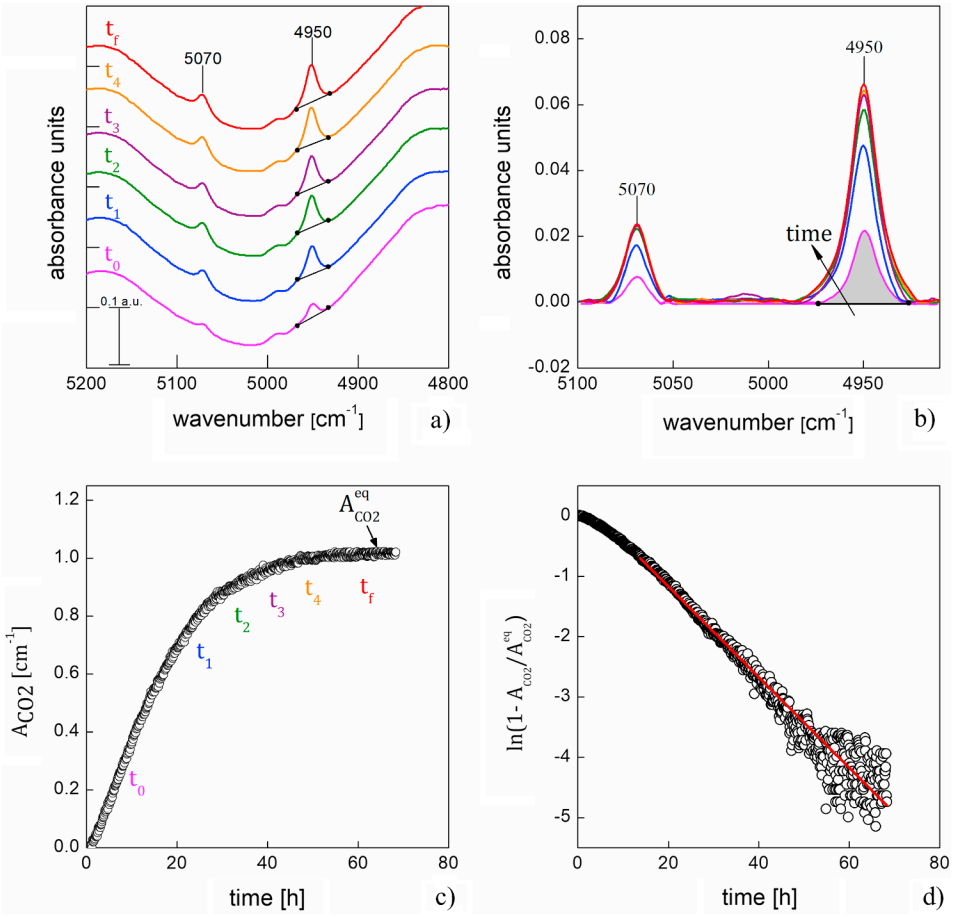

Fig. 3. CO_2 sorption monitoring in polyol at 4000 kPa and 35 °C: (a) time-evolution of FT-NIR spectra, (b) difference spectra, (c) integrated absorbance area A_{CO2} under the CO_2 combination band at 4950 cm^{-1} as a function of sorption time and (d) fit procedure to evaluate D by Eq. (1). The monitored A_{CO2} area is indicated in grey in (b) and the spectral acquisition time were: t_0 = 10 h; t_1 = 25 h; t_2 = 38 h; t_3 = 45 h; t_4 = 52 h; t_f = 60 h. In (a), spectra are shifted vertically for clarity.

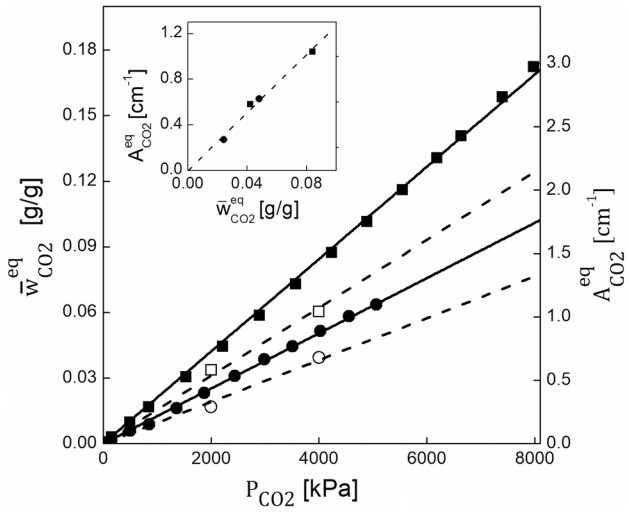

Fig. 4. Calibration of FT-NIR sorption in polyol (■) and PMDI (●). A^{eq}_{CO2} vs. P_{CO2} by FT-NIR (this study) (open symbols) and $\bar{w}^{eq}_{CO2}$ vs. P_{CO2} as measured by gravimetry-ADSA [15,16] (closed symbols) (A^{eq}_{CO2} vs. $\bar{w}^{eq}_{CO2}$ as inset). Lines are guide to the eye only.

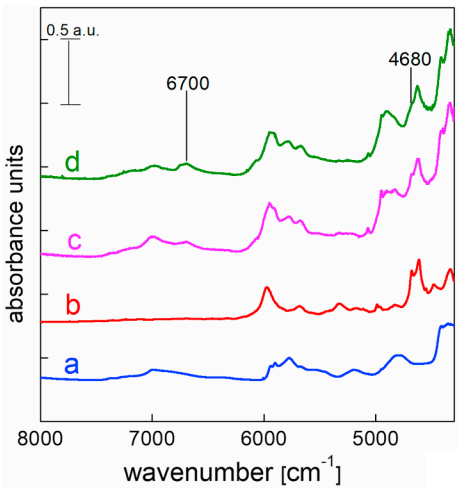

Fig. 5. FT-NIR spectra of the single reactants (polyol (a) and isocyanate (b)) collected before mixing (after 5 h of sorption time), spectra collected right after mixing the two components at 250 rpm for 10 s (c) and at the end of the curing reaction (d), at 35 °C and at CO_2 concentration of 0.05 g/g. Spectra are shifted vertically for clarity.

this specific case, average CO_2 weight fraction, $\bar{w}_{CO_2}$ = 0.05 g/g, was calculated by the procedure described in Section 2.2.2. Spectra reported in Fig. 5 show that the NCO band at 4680 cm^{-1}, characteristic of the PMDI, does not completely disappear at the end of the cure, proving its excess with respect to the polyol in the adopted formulation.

In Fig. 6 are reported details of the spectral regions of interest in this work and highlights time-evolution of characteristic signals. In particular, Fig. 6a shows the wavenumber range 5000–4400 cm^{-1}, where the NCO peak appears at 4680 cm^{-1}, while Fig. 6b shows the

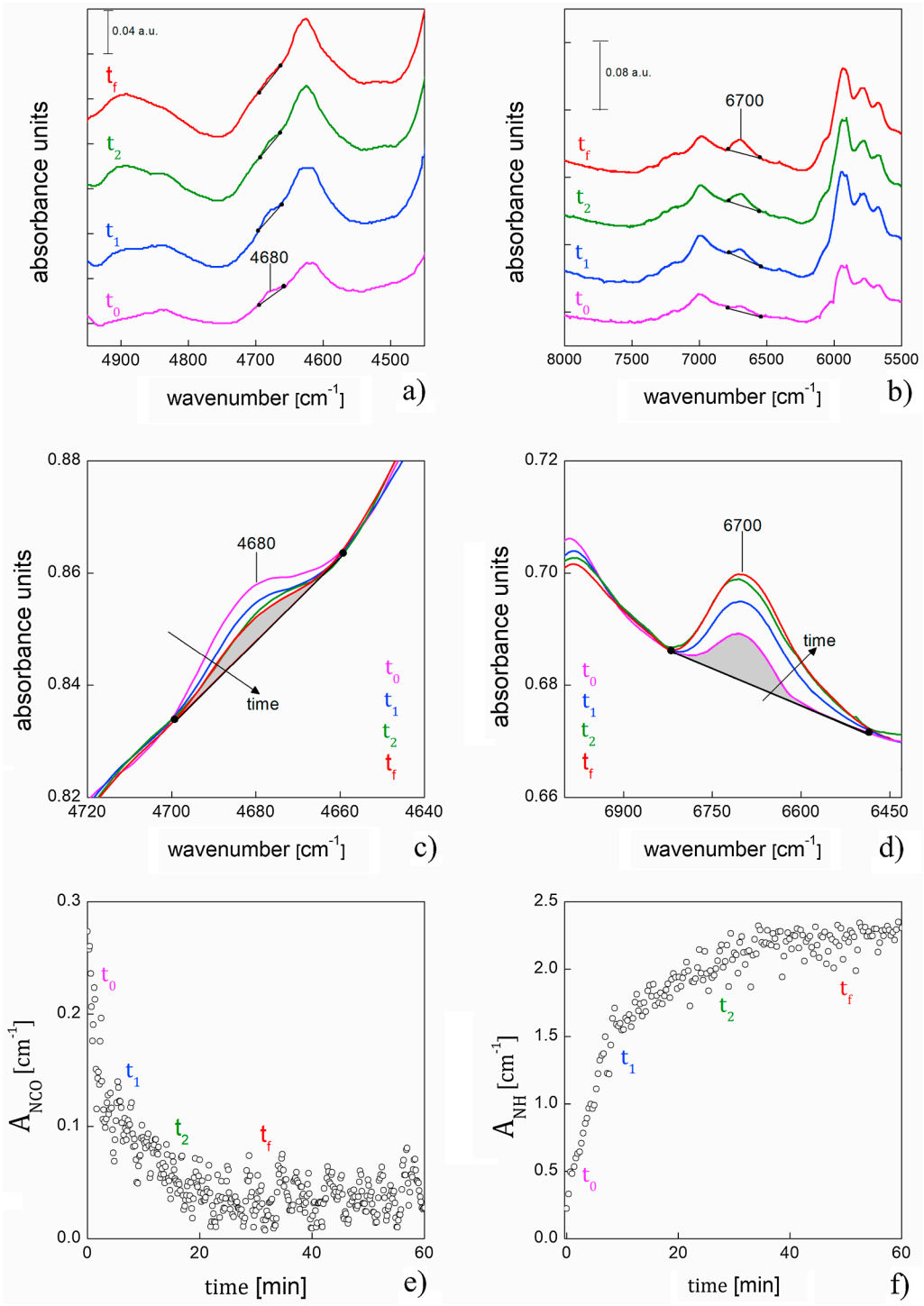

Fig. 6. Time-evolution of FT-NIR spectra (a and b), detail of the monitored peaks area (c and d) and integrated absorbance area of NCO (A_{NCO}) and NH (A_{NH}) bands (e and f) at 35 °C and at CO_2 concentration of 0.05 g/g. The monitored integrated areas are indicated in grey (c and d). Spectra at t_0 represent the beginning of reaction (after mixing), t_1 and t_2 are intermediate acquisitions (4 and 18 min for NCO band, 10 and 30 min for NH band), t_f represents the acquisition when the integrated area attains a constant value (ca. 33 and 57 min for NCO and NH bands, respectively). In (a) and (b), spectra are shifted vertically for clarity.

wavenumber range 8000–5500 cm^{-1}, where the NH peak appears at 6700 cm^{-1}. Correspondingly, Fig. 6c and d show in detail the monitored peaks area and Fig. 6e and f show the time evolution of A_{NCO} and A_{NH}, respectively.

The reaction rates can be described by various kinetic models. In particular, as typically done in the case of thermosetting polymers, we adopted a phenomenological model that describes both homogeneous processes and heterogeneous processes which are governed by phase-boundary reaction mechanisms [28,29], namely:

$$\frac{d\alpha}{dt} = k(1-\alpha)^n \tag{2}$$

where α is the time-dependent relative conversion ($\alpha = 1 - \frac{A_{NCO}}{A^0_{NCO}}$, where A^0_{NCO} is the initial absorbance area), $k = Ae^{-E_a/RT}$ is the Arrhenius-type kinetic constant and n represents the reaction order. Integration of Eq. (2) for n = 1 [29] yields:

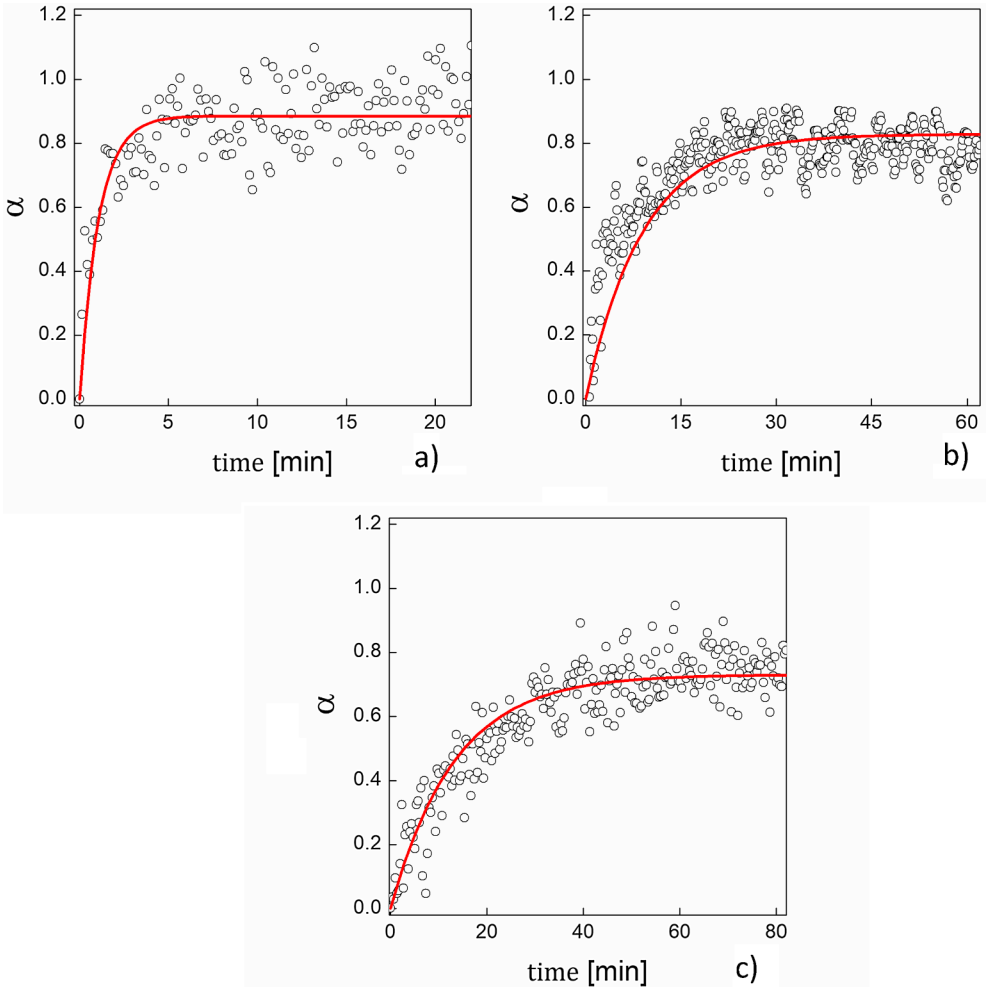

Fig. 7. NCO relative conversion (α) (at 4680 cm^{-1}) at 35 °C and (a) $\bar{w}_{CO_2}$ = 0g/g, (b) $\bar{w}_{CO_2}$ = 0.05g/g and (c) $\bar{w}_{CO_2}$ = 0.07g/g as function of reaction time. Open symbols are experimental data, lines are the fitting by Eq. (3).

$$\alpha = \alpha^f (1 - e^{-kt}) \quad (3)$$

Fig. 7 shows the results of the fitting of NCO conversion kinetics for selected $\bar{w}_{CO_2}$, evidencing the suitability of the selected simple model for the reaction kinetics, while the results of the fitting procedure (i.e. rate constant, k, and the final conversion α^f) are collectively reported in Table 3 for the whole range of investigated $\bar{w}_{CO_2}$. Kinetics data evidence a strong effect of $\bar{w}_{CO_2}$on the NCO consumption, with a minor effect on α^f.

The $\bar{w}_{CO_2}$ effect on the NCO consumption rate can be also evaluated by the conversion time, t_{c_NCO}, as the time needed to reach $0.95{\cdot}\alpha^f$, also reported in Table 3. It is possible to note that t_{c_NCO} increases monotonically with $\bar{w}_{CO_2}$, evidencing the slowing down of the PMDI conversion by CO_2. In particular, Fig. 8 shows the effect of $\bar{w}_{CO_2}$ on t_{c_NCO}, highlighting an apparent two-region process, with a decrease of the CO_2 effect above 0.07 g/g. Below this critical value of $\bar{w}_{CO_2}$ the slope of the t_{c_NCO} vs. $\bar{w}_{CO_2}$ curve is 927 ± 69 min.g/g, while at larger $\bar{w}_{CO_2}$ it is equal to 330 ± 40 min.g/g. This occurrence will be more thoughtfully investigated in the following.

As described above, the urethane formation, characteristic of the polyurethanes, is also readily observable by FT-NIR and the rise of the associated peak can be utilized to monitor the curing kinetics. As the urethane formation reaction involves the consumption of species involved in other reactions [27], it is easier to describe its kinetics in terms of the urethane characteristic group (NH) formation, instead of

Table 3
Effect of CO_2 on NCO conversion: results of the fitting procedure.

P_{CO2} [kPa]	CO_2 sorption time [hours]	$\bar{w}_{CO2}$[g/g]	k [min^{-1}]	α^f	t_{c_NCO} [min]
0	0	0	0.941 ± 0.056*	0.886 ± 0.043	4 ± 1
2000	5	0.025	0.126 ± 0.063	0.688 ± 0.13	24 ± 1.5
4000	5	0.050	0.110	0.828	45
6000	5	0.070	0.075 ± 0.009	0.731 ± 0.036	70 ± 2
7000	5	0.085	0.066 ± 0.005	0.771 ± 0.14	80 ± 1
7500	5	0.090	0.065	0.941	82
8000	5	0.100	0.063	0.863	84
10,000	5	0.120	0.059	0.767	90
12,000	5	0.140	0.056	0.595	95

* Where reported, standard deviations were evaluated on experiments performed in triplicate.

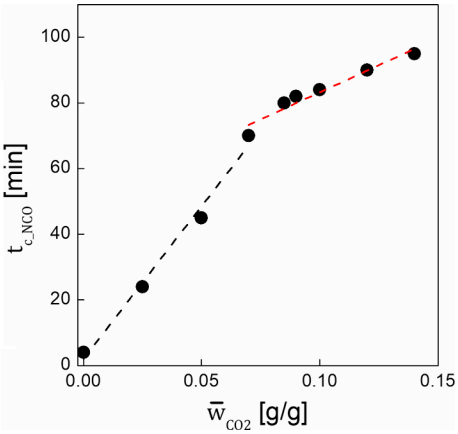

Fig. 8. NCO conversion time (t_{c_NCO}) at different $\bar{w}_{CO_2}$. Lines are only guide to the eye.

reactants consumption (conversion). The assumptions adopted to derive the simple kinetic model of Eq.2, in this case yield:

$$A_{NH} = A^{f}_{NH}(1 - e^{-kt}) \quad (4)$$

where A_{NH} is the integrated absorbance area of the NH peak at time t, and A^{f}_{NH} is the integrated absorbance area final value ($A^{0}_{NH} = 0$, as no urethane is in the system at time t = 0) [30]. In this case, it is more appropriate to express the degree of curing by normalizing with respect to the final A^{f}_{NH}, as follows:

$$X(t) = \frac{A_{NH}}{A^{f}_{NH}} = (1 - e^{-kt}) \quad (5)$$

Table 4
Effect of CO_2 on NH formation: results of the fitting procedure.

P_{CO2} [kPa]	CO_2 sorption time [hours]	$\bar{w}_{CO2}$[g/g]	k [min^{-1}]	t_{c_NH} [min]
0	0	0	0.735 ± 0.025*	5.6 ± 0.6
2000	5	0.025	0.162 ± 0.001	28.5 ± 3.5
4000	5	0.050	0.102	57
6000	5	0.070	0.076 ± 0.016	73.5 ± 3.5
6000	12	0.079	0.063	77
10,000	1.5	0.079	0.065	79
7000	5	0.085	0.066 ± 0.006	81 ± 2
7500	5	0.090	0.062	83
8000	5	0.100	0.063	87
10,000	5	0.120	0.056	95
12,000	5	0.140	0.050	103

* Where reported, standard deviations were evaluated on experiments performed in triplicate

The experimental data and fitting by eq. (4), for selected $\bar{w}_{CO_2}$ are reported in Fig. 9, while the results of the fitting procedure are reported in Table 4.

Fig. 10 collects all of the reaction kinetics fitting curves at the different $\bar{w}_{CO2}$ highlighting the important slowing down effect by the CO_2

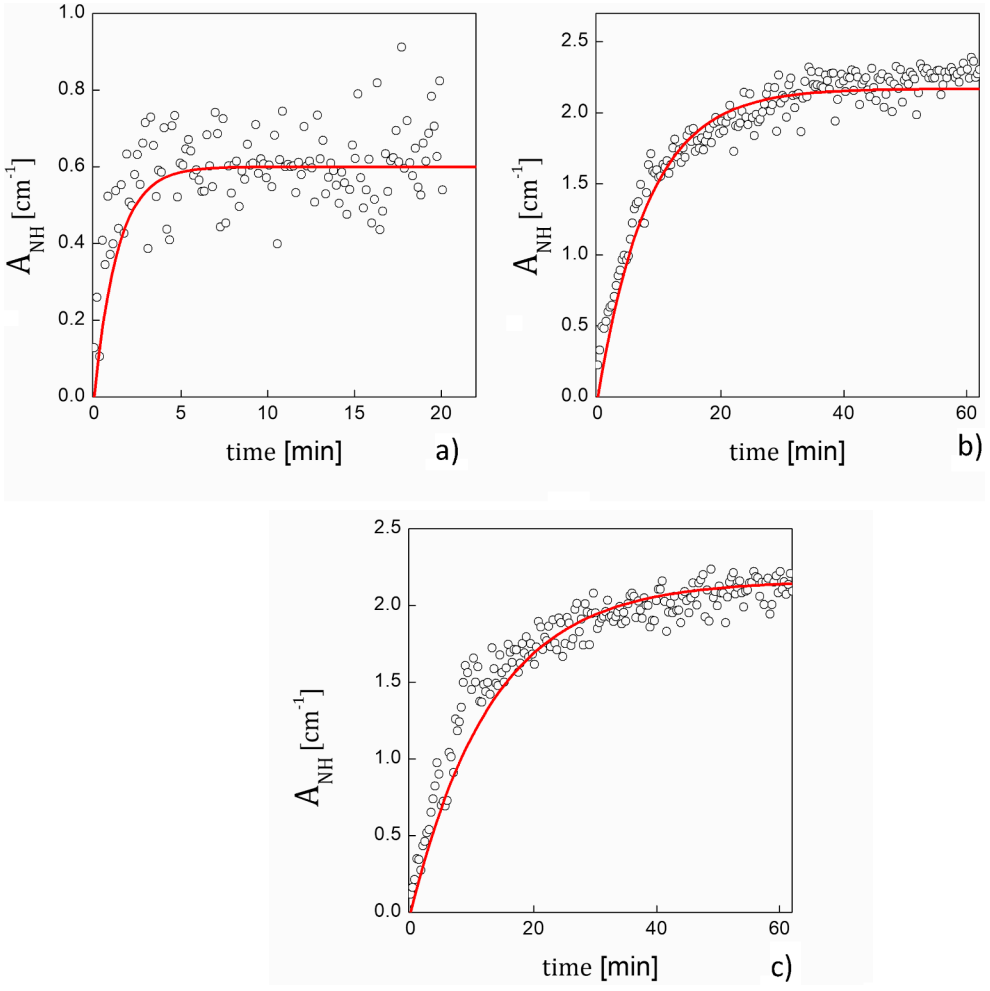

Fig. 9. NH integrated absorbance area (A_{NH} - at 6700 cm^{-1}) at 35 °C and (a) $\bar{w}_{CO_2}$ = 0g/g, (b) $\bar{w}_{CO_2}$ = 0.05g/g and (c) $\bar{w}_{CO_2}$ = 0.07g/g as function of reaction time. Open symbols are experimental data, lines are fitting by Eq. (5).

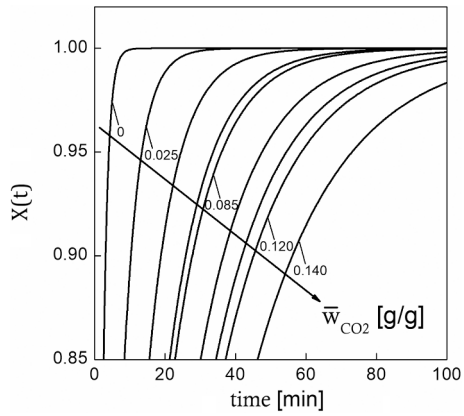

Fig. 10. Degree of curing X(t) of PUs reacted at different $\bar{w}_{CO2}$ evaluated as a function of the reaction time. Line represents the fitting of experimental data by Eq. (5).

on PU synthesis.

The $\bar{w}_{CO_2}$ effect on the NH formation rate can be also evaluated by the formation time, t_{c_NH}, as the time needed to reach 0.95·X (Fig. 11a). It is possible to note that t_{c_NH} increases monotonically with $\bar{w}_{CO_2}$. An interesting question that may arise from these data regards the role of the CO_2 pressure and its supercritical transition. To this aim, we performed additional tests in which the same $\bar{w}_{CO_2}$ is achieved at two different pressures, specifically below and above the critical pressure. Achieving the same $\bar{w}_{CO_2}$ at two different pressures can be easily done by adjusting the sorption time as reported in Section 2.2.2. In particular, Table 4 shows that $\bar{w}_{CO_2}$ = 0.079 g/g can be achieved after solubilization at 10000 kPa for 1.5 h or at 6000 kPa for 12 h. Fig. 11b and data reported in Table 4 rule out the effect of the supercritical transition and clarifies that, in our case, the controlling variable on the polyurethane synthesis is the $\bar{w}_{CO_2}$, not P_{CO2}, as t_{c_NH} does not change with P_{CO2} (open symbols in Fig. 11b), at constant $\bar{w}_{CO_2}$.

As in the case of Fig. 8 (for the NCO conversion), Fig. 11a confirms the apparent two-stage process, with a decrease of the CO_2 effect above 0.07 g/g. Catalyst deactivation [5,7] as well as dilution effects [31,32] have been reported in the underlying literature. With reference to the former, in the specific case of catalyst deactivation by CO_2, it has been reported, for instance, a reaction between CO_2 and 1,8-diazabicyclo [5.4.0]undec-7-ene (DBU) tertiary amine in 1-hexanol and 1-propanol [7]. The mixture of amidine base and the alcohol reacts with CO_2 to form a high polarity ionic liquid with quaternary ammonium cations and alkylcarbonate anions. In our case, catalyst deactivation can be likewise due to the Lewis acid-base interaction between CO_2, polyol and tertiary amines (the catalytic species in the formulation under study). With reference to the dilution effect, a traditional physical chemistry description of such a reacting system would be of a diffusion-controlled one, where reactant molecules have to jostle their way through the solvent but, when in contact, stay near each other for much longer, in the so-called "cage effect". In our case, the swelling induced by CO_2 sorption in the two phases (the polyol [15] and PMDI [16]) results in a decrease of reactant concentration and a corresponding decrease of reaction rate [32]. Here, we may speculate that both catalyst deactivation and dilution mechanisms are occurring concurrently, up to a complete saturation of the catalytic sites by CO_2 at 0.07 g/g in this specific case. At higher $\bar{w}_{CO_2}$, the sole diluting effect emerges. At $\bar{w}_{CO_2}$ below 0.07 g/g both mechanisms concur to the effect of $\bar{w}_{CO_2}$ on t_{c_NH}, linearly increasing with a slope of 990 ± 39 min.g/g in the 0–0.07 range, while at larger $\bar{w}_{CO_2}$, catalyst deactivation mechanism fades due to saturation of catalytic sites by CO_2 and only the dilution effect is active, with a corresponding reduced slope of the t_{c_NH} vs. $\bar{w}_{CO_2}$ curve equal to 414 ± 10 min.g/g.

To prove this hypothesis and to separate the catalyst deactivation effect from the dilution effect, further tests were performed on a polyol-PMDI formulation in which no catalysts were included. Obviously, in this case both t_{c_NCO} and $t_{c_NH}$are expected to increase with respect to the case of the formulation with the catalyst. Here, the effect of CO_2 on reaction kinetics would be solely due to the dilution effect, and should maintain a similar dependence of the high-$\bar{w}_{CO_2}$ behavior of the catalyzed formulations. This is indeed the case, as reported in Fig. 12, where a comparison is drawn between the catalyzed and non-catalyzed formulations, in terms of the effects of $\bar{w}_{CO_2}$ on t_{c_NCO} and t_{c_NH} (Fig. 12a and b, respectively). Operating conditions and kinetics fitting results are reported, for the non-catalyzed formulation, in Table 5.

In the case of the non-catalyzed formulation, the slope of the t_{c_NCO} vs. $\bar{w}_{CO_2}$ curve is 300 ± 46 min.g/g, while for the t_{c_NH} vs. $\bar{w}_{CO_2}$ curve it is 400 ± 23 min.g/g. Of course, as there is no catalyst to deactivate, there is no threshold $\bar{w}_{CO_2}$ value, in this case. Comparison of the slopes of the formulation with catalysts above the catalyst deactivation critical value of $\bar{w}_{CO_2}$, equal to 330 ± 40 and 414 ± 10, respectively for t_{c_NCO} and t_{c_NH} seems a good proof of the proposed two concurring mechanisms. It is worth of note, here, that no foaming occurred during the testing as the vessel was slowly pressure vented long after the curing reaction has gone to completion. For this reason, after each curing kinetics experiment at several CO_2 pressures and 35 °C, the sample was always a compact PU product with high, bulk density. Further studies

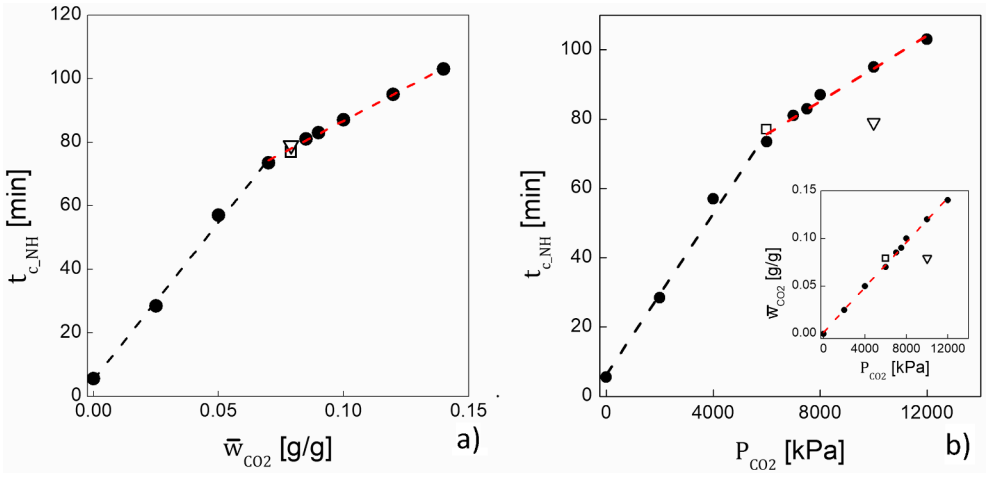

Fig. 11. Effect of CO_2 on t_{c_NH}; data reported as a function of (a) $\bar{w}_{CO_2}$ and (b) P_{CO2} ($\bar{w}_{CO_2}$ vs. P_{CO2} as inset). Symbols are experimental data, lines are only guide to the eye. Open symbols refer to tests performed at $\bar{w}_{CO_2}$ achieved after sorption conducted at different pressures (by adapting the sorption time): test conducted at 6000 kPa and 12 h of sorption (□), test conducted at 10000 kPa and 1.5 h of sorption (▽).

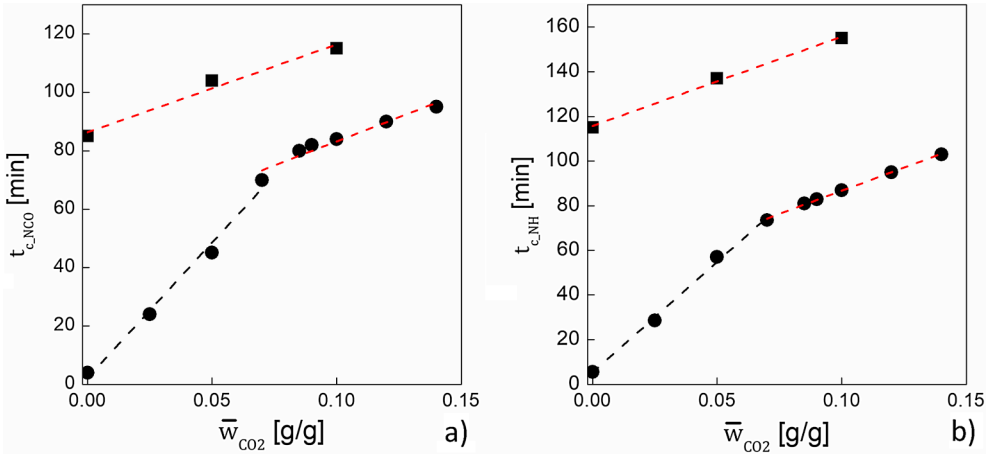

Fig. 12. Effect of CO_2 on (a)t_{c_NCO} and (b) t_{c_NH}. Round and square symbols are experimental data for formulations with and no catalyst respectively, lines are only guide to the eye.

Table 5
Effect of CO_2 on t_{c_NCO} and t_{c_NH}: results of the fitting procedure.

P_{CO2} [kPa]	CO_2 sorption time [hours]	$\bar{w}_{CO2}$ [g/g]	t_{c_NCO} [min]	t_{c_NH} [min]
0	0	0	85	115
4000	5	0.050	104	137
8000	5	0.100	115	155

have to be conducted for detailed interpretation and modeling of such a complex diffusion controlled reacting system. These studies can rely on the availability of phases compositions, mutual diffusivities, degree of swelling [15,16] and viscosities of the species involved in the reactions, which, to our point of view, represent a unique, rich set of data.

4. Conclusions

Carbon dioxide sorption in polyol/PMDI system, under high-pressure, was studied by in situ near infrared spectroscopy. A kinetic analysis was performed on the polyurethane reacting system, at 35 °C and still under CO_2 pressure (up to 12000 kPa) and characteristic urethane (NH group) and PMDI (NCO group) bands were monitored. Results revealed, in the investigated experimental range, a significant slowing down effect of the sorbed CO_2, apparently with two mechanisms: i) the catalyst deactivation due to a reaction of tertiary amines with CO_2 and the polyol and ii) the dilution effect due to swelling by CO_2 sorption in the two reacting phases. Above a weight fractions of ca. 0.07 g/g, where, apparently, catalytic sites were saturated by CO_2, only the swelling by CO_2 further contributed to the slowing down of the reaction kinetics. This effect has been confirmed by testing a PU formulation without catalysts. Finally, it has been proved that the sorbed CO_2 weight fraction is, in fact, responsible for the observed effects, not the pressure. In particular, apparently, the transition to the supercritical state of the outer CO_2 in contact with the polymeric phases is not relevant to the reactions analyzed in this work.

Acknowledgments

The financial support of the European Union's (LIFE13-EN/IT/001238 project, http://ec.europa.eu/environment/life; www.dow.com/k12) is gratefully acknowledged.

Appendix A. Supplementary material

Supplementary data to this article can be found online at https://doi.org/10.1016/j.eurpolymj.2019.03.047.

References

[1] D. Randall, S. Lee, Blowing agents, in The polyurethanes book, John Wiley & Sons Inc, New Jersey, 2003, pp. 127–136.
[2] S. Costeux, CO_2-Blown Nanocellular Foams, J. Appl. Polym. Sci. 131 (2014) 41293, https://doi.org/10.1002/app.41293.
[3] Dow Italia S.r.l., LIFE 13 ENV/IT/001238 < http://ec.europa.eu/environment/life/project/Projects/index.cfm?fuseaction=search.dspPage&n_proj_id=5077 > .
[4] F. Stassin, R. Jérôme, Effect of pressure and temperature upon tin alkoxide-promoted ring-opening polymerisation of ε-caprolactone in supercritical carbon dioxide, Chem. Commun. (2002) 232–233, https://doi.org/10.1039/b209170d.
[5] H. Tiltscher, H. Wolf, H. Schelchshorn, Utilization of supercritical fluid solvent-effects in heterogeneous catalysis, Ber. Bunsen Ges. Phys. Chem. 88 (1984) 897–900, https://doi.org/10.1002/bbpc.19840880926.
[6] P.G. Jessop, S.M. Mercer, D.J. Heldebrant, CO_2-triggered switchable solvents, surfactants, and other materials, Energy Environ. Sci. 5 (2012) 7240–7253, https://doi.org/10.1039/c2ee02912j.
[7] P.G. Jessop, D.J. Heldebrant, X. Li, C.A. Eckert, C.L. Liotta, Reversible nonpolar-to-polar solvent, Nature. 436 (2005) 1102, https://doi.org/10.1038/nature4361101a.
[8] M.L. Pinto, L. Mafra, J.M. Guil, J. Pires, J. Rocha, Adsorption and activation of CO_2 by amine-modified nanoporous materials studied by solid-state NMR and $^{13}CO_2$ adsorption, Chem. Mater. 23 (2011) 1387–1395 https://pubs.acs.org/doi/10.1021/cm1029563.
[9] P.N. Sutar, A. Jha, P.D. Vaidya, E.Y. Kenig, Secondary amines for CO_2 capture: a kinetic investigation using N-ethylmonoethanolamine, Chem. Eng. J. 207–208 (2012) 718–724, https://doi.org/10.1016/j.cej.2012.07.042.
[10] Y.G. Ko, S.S. Shin, U.S. Choi, Primary, secondary, and tertiary amines for CO_2 capture: designing for mesoporous CO_2 adsorbents, J. Colloid Interface Sci. 361 (2011) 594–602, https://doi.org/10.1016/j.jcis.2011.03.045.
[11] A. Furstner, G. Seldel, N. Kindler, Macrocycles by ring-closing-Metathesis, XI: syntheses of (R)-(+)-lasiodiplodin Zeranol and Truncated Salicylihalamides, Tetrahedron 55 (1999) 8215–8230, https://doi.org/10.1016/S0040-4020(99)00302-6.
[12] K. Wittmann, W. Wisniewski, R. Mynott, W. Leitner, C.L. Kranemann, T. Rische, P. Eilbracht, S. Kluwer, J.M. Ernsting, C.J. Elsevier, Supercritical carbon dioxide as solvent and temporary protecting group for rhodium-catalyzed hydroaminomethylation, Chem. Eur. J. 7 (2001) 4584–4589.
[13] J. Xiong, D.Li, J. Zhang, D.H.F. Guo, B. Wang, W. Liu, Surfactants For Polyurethane Foams, Patent WO/2016/095128, Midland, Michigan, 2016.
[14] Z. Yang, T. Liu, D. Hu, Z. Xu, L. Zhao, Foaming window for preparation of microcellular rigid polyurethanes using supercritical carbon dioxide as blowing agent, J. Supercrit. Fluids 147 (2019) 254–262, https://doi.org/10.1016/j.supflu.2018.11.001.
[15] M.R. Di Caprio, G. Dal Poggetto, M.G. Pastore Carbone, E. Di Maio, S. Cavalca, V. Parenti, S. Iannace, Polyether polyol/CO_2 solutions: Solubility, mutual diffusivity, specific volume and interfacial tension by coupled gravimetry-axisymmetric drop shape analysis, Fluid Phase Equilib. 425 (2016) 342–350, https://doi.org/10.1016/j.fluid.2016.06.023.
[16] M.R. Di Caprio, B. Immirzi, E. Di Maio, S. Cavalca, V. Parenti, S. Iannace, G. Mensitieri, Mass transport and physical properties of polymeric methylene diphenyl diisocyanate/CO_2 solutions, Fluid Phase Equilib. 456 (2018) 116–123, https://doi.org/10.1016/j.fluid.2017.10.018.
[17] M.R. Di Caprio, D. Tammaro, E. Di Maio, S. Cavalca, V. Parenti, A. Fangareggi, S. Iannace, A pressure vessel for studying gas foaming of thermosetting polymers: sorption, synthesis and processing, Polym. Test. 62 (2017) 137–142, https://doi.org/10.1016/j.polymertesting.2017.06.019.
[18] T. Guadagno, S.G. Kazarian, High-pressure CO_2-expanded solvents: simultaneous measurement of CO_2 sorption and swelling of liquid polymers with in-situ near-IR spectroscopy, J. Phys. Chem. 108 (2004) 13995–13999, https://doi.org/10.1021/

jp0481097.
[19] M.G. Pastore Carbone, E. Di Maio, S. Iannace, G. Mensitieri, Simultaneous experimental evaluation of solubility, diffusivity, interfacial tension and specific volume of polymer/gas solutions, Polym. Test. 30 (2011) 303–309, https://doi.org/10.1016/j.polymertesting.2011.01.004.
[20] A. Al Nabulsi, D. Cozzula, T. Hagen, W. Leitner, T.E. Muller, Isocyanurate formation during rigid polyurethane foam assembly: a mechanistic study based on in situ IR and NMR spectroscopy, Polym. Chem. 9 (2018) 4891–4899, https://doi.org/10.1039/C8PY00637G.
[21] J. Dupuy, S. Benali, A. Maazouz, G. Lachenal, D. Bertrand, FT-NIR monitoring of a scattering polyurethane manufactured by reaction injection molding (RIM): univariate and multivariate analysis versus kinetic predictions, Macromol. Symp. 184 (2002) 249–260, https://doi.org/10.1002/1521-3900(200208)184 1 < 249::AID-ASY249 > 3.0.CO;2-5.
[22] J. Crank, The Mathematics of diffusion, second ed., Oxford University Press, Bristol, England, 1975.
[23] C. Wenning, S. Barbe, D. Achten, A.M. Schmidt, M.C. Leimenstoll, Prediction of initial miscibility for ternary polyurethane reaction mixtures on basis of solubility parameters and flory-huggins theory, Macromol. Chem. Phys. 219 (2018) 1700544, https://doi.org/10.1002/macp.201700544.
[24] M. Buback, J. Schweer, H. Tups, Near Infrared absorption of pure carbon dioxide up to 3100 bar and 500 k. I. wavenumber range 3200 cm^{-1} to 5600 cm^{-1}, Z. Naturforsch., A: Phys. Sci. 41 (1986) 505–511, https://doi.org/10.1515/zna-1986-0308.
[25] P. La Manna, P. Musto, G. Galli, E. Martinelli, In situ FT-IR spectroscopy investigation of the water sorption of amphiphilic PDMS crosslinked Networks, Macromol. Chem. Phys. 218 (2017) 1600585, https://doi.org/10.1002/macp.201600585.
[26] C.M. Balik, On the extraction of diffusion coefficients from gravimetric data for sorption of small molecules by polymer thin films, Macromolecules 29 (1996) 3025–3029, https://doi.org/10.1021/ma9509467.
[27] D. Randall, S. Lee, Outline of polyurethane chemistry, The polyurethanes book, John Wiley & Sons Inc, New Jersey, 2003, pp. 113–126.
[28] A.E. Venger, Y.E. Fraiman, F.B. Yurevich, Applicability of one-stage chemical reaction kinetic equation to describe non-isothermal destruction processes, J. Therm. Anal. 27 (1983) 325–331, https://doi.org/10.1007/BF01914669.
[29] G. Carotenuto, L. Nicolais, Kinetic study of phenolic resin cure by IR spectroscopy, J. Appl. Polym. Sci. 74 (1999) 2703–2715, https://doi.org/10.1002/(SICI)1097-4628(19991209)74:11 < 2703::AID-APP18 > 3.0.CO;2-M.
[30] G. Ragosta, M. Abbate, P. Musto, G. Scarinzi, Spectroscopic, mechanical and dynamic-mechanical studies on the photo-aging of a tetrafunctional epoxy resin, Macromol. Symp. 286 (2009) 34–41, https://doi.org/10.1002/masy.200951204.
[31] J.M. DeSimone, W. Tumas, Green chemistry using liquid and supercritical carbon dioxide, Oxford University Press, New York, 2003.
[32] P. Atkins, J. de Paula, Molecular reaction dynamics, in Atkins' physical chemistry, eighth ed., Oxford University Press, Oxford, England, 2006, pp. 869–908.